International Immunopharmacology 75 (2019) 105755

Contents lists available at ScienceDirect

International Immunopharmacology

journal homepage: www.elsevier.com/locate/intimp

Therapeutic effects of Nimbolide, an autophagy regulator, in ameliorating pulmonary fibrosis through attenuation of TGF-β1 driven epithelial-to-mesenchymal transition

M. Prashanth Goud[1], Swarna Bale[1], Gauthami Pulivendala, Chandraiah Godugu*

Department of Regulatory Toxicology, National Institute of Pharmaceutical Education and Research (NIPER), Balanagar, Hyderabad, Telangana 500037, India

A B S T R A C T

Pulmonary fibrosis is an irreversible lung disorder with predictable decline in lung function leading to respiratory insufficiency. Incidence of pulmonary fibrosis has been apparently increasing worldwide. Though aetiology of this disease remains unclear, potential roles of infection, disordered cell biology, genetic influence etc. have been proposed. Pirfenidone and nintedanib are the only two US FDA approved drugs to treat pulmonary fibrosis. Autophagy is a catabolic intracellular pathway that plays a crucial role in maintaining cellular homeostasis, which is involved in many disorders including fibrotic diseases. The present study investigated the role of Nimbolide, an important active constituent of Neem in TGF-β1 induced *in vitro* and bleomycin induced *in vivo* model of pulmonary fibrosis, with a slight emphasis on regulation of fibrosis related autophagy. Protein expression studies showed significant reduction in mesenchymal, fibrotic markers and a substantial up regulation of epithelial markers upon treatment with Nimbolide. Nimbolide regulated autophagy signaling by dampening LC-3 and p-62 expression and increasing Beclin 1 expression as evidenced by immunohistochemistry and confocal microscopy. Our study demonstrates Nimbolide as a potent anti-fibrotic agent and its ability to regulate fibrosis associated autophagy.

1. Introduction

Idiopathic pulmonary fibrosis (IPF) also known as cryptogenic fibrosing alveolitis is a chronic, progressive parenchymal lung disease which involves inappropriate formation of scar tissue, relentless accumulation of extracellular matrix (ECM) in the lungs and remodelling of lung architecture [1,2]. IPF is the most common form of interstitial fibrosis which manifests as dyspnoea, cough, digital clubbing etc. [3]. Pathobiological mechanisms of IPF are quite nebulous, supervised by multiple factors which lead to irreversible loss of pulmonary function [1,4]. Despite transient clinical stability, progressive deterioration is inevitable which forms the grounds for its poor prognosis with a direful median survival rate of approximately 3 years [5,6].

Briefing the histological aspects, chronic epithelial injury by various insultants trigger transforming growth factor (TGF-β1) mediated cellular transition from normal epithelium to mesenchymal like state [7]. Ligand-activated TGF-β1 receptor type II (TGFβRII) signals through Smad-dependent (canonical) and Smad-independent (noncanonical) pathways. TGF-β1 mediates the conversion of fibroblast to myofibroblasts, thus induces enhanced motility and aberrantly up regulates the expression of fibrotic genes [8]. In TGF-β1/Smad canonical pathway, phosphorylated Smad2/3 binds to Smad4 which translocates into the nucleus. Smad2/3/4 complex regulates components of a pivotal set of transcriptional regulators which are responsible to coordinate processes in the mesenchymal cell state change and ECM deposition [9]. PF is a fatal fibrotic disease characterized by unhampered proliferation and persistence of fibroblasts [2]. This is followed by formation of hallmarks of IPF, fibroblast and myofibroblast foci which secrete excessive ECM [10].

Autophagy is a self-degradative evolutionarily conserved catabolic intracellular process for degradation of cellular cytoplasmic cargo, long lived proteins and mitochondria to maintain homeostasis. This lysosomal degradative pathway is accomplished through sequestering cytoplasmic material in double membraned autophagosomes [11]. Though known to be a process propitious to the cell's well-being, growing body of evidences underscore autophagy to be a cornerstone in the pathogenesis of many disorders including fibrosis contrary to the conventional notion [12]. Committed research in the arena of autophagy in the past decade has revealed intriguing details about the mechanistic role of autophagy in disease which captivates further exploration of its role in pulmonary fibrosis [13,14].

Natural compounds are often neglected for treatment of pulmonary fibrosis. One such barely investigated molecule is Nimbolide (NIM), a tetranortriterpenoid limonoid from leaves and flowers of Neem tree (*Azadirachta indica*). Despite multiple compounds being isolated from neem including azadirachtin, salannin, nimbin and nimbic acid,

* Corresponding author.
E-mail address: chandragodugu@gmail.com (C. Godugu).
[1] Equal contribution.

https://doi.org/10.1016/j.intimp.2019.105755
Received 18 June 2019; Received in revised form 5 July 2019; Accepted 10 July 2019
Available online 01 August 2019
1567-5769/ © 2019 Elsevier B.V. All rights reserved.

Nimbolide is the major active compound eliciting a wide array of biological functions like anti-proliferative, anti-cancer, anti-malarial etc. [15,16]. NIM is a molecule with β-unsaturated system and δ-lactonic ring, possessing interesting properties. It is known to have diverse molecular targets which include growth factors and their receptors, transcription factors, protein kinases and genes regulating cell proliferation and apoptosis etc. [17]. Of note, NIM was recently proven to be inhibitor of epithelial-to-mesenchymal-transition (EMT) [18]. Additionally, NIM has been proven to be an inhibitor of PI3K/Akt signaling cascade and MAPK signaling [19], thus demonstrating its diversified interaction with major signaling pathways and their receptors. This study is aimed at evaluating the efficacy of NIM in TGF-β1 induced *in vitro* and Bleomycin (BLM) induced *in vivo* pulmonary fibrosis.

2. Materials & methods

2.1. Chemicals, reagents and antibodies

Nimbolide was purchased from Aptus Laboratories (Hyderabad, India). Recombinant human TGF-β1 was purchased from Biolegend (San Deigo, USA). Bleomycin sulphate was procured from Cipla labs (Mumbai, India), chloramine-T, Trans-L-Hydroxyproline, Ehrlich reagent, reduced glutathione (GSH), 5,5-dithio-bis(2-nitrobenzoic acid) (DTNB), 2-thiobarbituric acid (TBA), bovine serum albumin (BSA), sodium dodecyl sulphate (SDS), glacial acetic acid, sodium nitrite, Bradford reagents, monodansylcadavarine, chloroquine and acridine orange were purchased from Sigma Aldrich. Antibodies were procured from Sigma Aldrich, Santa Cruz Biotechnologies and Cell Signaling Technology. IL-1β, TNF-α and IL-6 ELISA kits were purchased from e-Biosciences, USA. All other chemicals used in this study were obtained commercially and were of analytical grade.

2.2. Cell culture

HFL 1 cells were procured from ATCC (ATCC® CCL153™) and A549 were purchased from National Centre for Cell Science (NCCS, Pune, India). A549 cells were cultured using RPMI media supplemented with 10% Fetal Bovine Serum (FBS) and 1% antibiotic solution (Invitrogen, USA). HFL 1 cells were cultivated in F12K medium with 10% FBS. All the cells were maintained in a humidified atmosphere of 95% air and 5% CO2. Human recombinant TGF-β1 at a concentration of 10 ng/mL was used as a fibrotic inducer. NIM was dissolved in DMSO to prepare a stock solution of 10 mM and was diluted suitably to obtain required concentrations before experimentation. The concentration of DMSO for all assays did not exceed 0.1%. To investigate the probable pathways altered upon treatment with pharmacological intervention under scrutiny, cells were pre-incubated with 0.5, 1 and 2 μM NIM for 2 h followed by TGF-β1 induction for 24 h.

2.3. Cell viability by MTT assay

Effect of NIM on cell viability of HFL 1 and A549 cells was determined by MTT assay (3-(4,5-dimethylthiazol-2-yl)-2,5-diphenyltetrazolium bromide) [43]. Briefly, cells were cultured in 96-well plate at a density of 5×10^3 cells per well. After reaching enough confluency, cells were treated with NIM; 24 h post treatment, MTT solution at a concentration of 0.5 mg/mL was added and incubated for 4 h followed by addition of DMSO to solubilise formazan crystals. After 20 min incubation post addition of DMSO, the absorbance was measured using a multi-mode spectrophotometer at 570 nm. Experiments were performed in triplicates and data was expressed as percentage cell viability *versus* concentration of the compound by taking control cells as 100% viable cells.

2.4. Cell migration assay

Cell migration assay on HLF 1 cells was performed by seeding cells at a density of 1×10^5 in a 6 well plate. After enough confluency was attained, an artificial wound was created by disrupting the cell monolayer with a sterile 10 μL tip across the centre of the well. Wells were washed sufficiently to remove detached cells and were treated with TGF-β1 and NIM at concentrations of 0.5, 1 and 2 μM accordingly after replacing wells with fresh serum free media. Representative photographs of the gap created were captured by microscope at 0 and 24 h post incubation and were quantitatively evaluated using imageJ software [43].

2.5. MDC staining

MDC staining is considered as a specific marker for detection of autophagic vacuoles. Briefly, cells were grown on cover slips placed in 6 well plate. When desired confluency was attained, the cells were treated with 2 μM of NIM with or without TGF-β1 at a concentration of 10 ng/mL. 24 h post treatment, cells were treated with MDC at a concentration of 0.05 mM in PBS and incubated at 37 °C for 1 h for allowing autophagic vacuoles to be labelled. After incubation, the cells were washed thrice with PBS and representative images were captured using confocal microscope [44].

2.6. Acridine orange staining

HFL 1 cells were grown in sterile 6 well plate till desired confluency was acquired. Cells were then treated with 2 μM of NIM with or without TGF-β1 at a concentration of 10 ng/mL for 24 h. Post treatment, cells were stained with acridine orange (1 mg/mL) for 15 min. Acridine orange solution was removed and representative micrographs were captured using fluorescent microscope.

2.7. Experimental animals and grouping

Male Swiss mice (8–9 week old) were purchased from Teena Labs, Hyderabad, India. Animals were housed as four per cage, maintained under 12:12 h light and dark conditions at 25 °C, were allowed free access to food and water. Animals were acclimatized for at least one week before starting the experiments. All the animal experimentations in this study were approved by institutional animal ethics committee (IAEC), NIPER-Hyderabad and were performed in accordance with guidelines and regulations of Committee for the purpose of control and supervision of experiments on animals (CPCSEA), Govt. of India. Mice ($n = 8$) were divided into: i) Normal control (0.9% *w/v* saline, intraperitoneally), ii) BLM control (2 U/kg, oropharyngeally), iii) BLM + NIM low dose (100 μg/kg), iv) BLM + NIM High dose (300 μg/kg) and v) NIM control (300 μg/kg). NIM was administered intraperitoneally, once daily for 21 days.

2.8. Lung-body weight index

Animal body weights were recorded every third day in the 21 day study. On the last day of study, animals were euthanized humanely by using 5% CO_2, lungs were harvested, cleaned in PBS and weight of the lungs was recorded. Lung weight index was calculated as ratio of the lung weight to the body weight.

2.9. Bronchoalveolar lavage (BAL) biochemical parameters

Animals were euthanized using 5% Isoflurane followed by tracheaostomy for BAL collection. BAL fluid (BALF) was collected by passing ice-cold PBS (1.5 mL each time, thrice) into the trachea, followed by gentle aspiration of PBS by inserting a catheter into the trachea. The percentage recovery of lavage fluid was approximately 85%

and significantly did not differ among the animal groups. BALF was pooled and subjected to total cell count and differential cell count using Siemens hematology system (Advia 2120i). The collected BAL fluid was centrifuged and the supernatant was stored at -80° C for further experimentation.

(a) Lactate dehydrogenase (LDH) level measurement level measurement

BAL fluid LDH levels were estimated as a biomarker of cell lung injury. LDH in BALF from all the animal groups were measured calorimetrically at 340 nm as per instructions of a commercially available kit Accurex (Mumbai, India). Results were expressed as IU/L.

(b) Total protein concentration

Total protein content in BALF was determined using Bradford method, measured spectrophotometrically at 595 nm. Results were expressed as mg/ml of BALF protein.

2.10. Tissue biochemical parameters

(a) Determination of Glutathione content (GSH)

Glutathione levels were measured using Ellmans reagent [5, 5′-dithiobis-2-nitro benzoic acid (DTNB) solution] [45]. Ellmans reagent was added to supernatants of whole lung tissue containing GSH buffer, incubated for 5 min in dark and absorbance was measured at 412 nm. Values obtained were compared with series of reduced glutathione standards. Results were expressed as μM/mg of lung protein.

(b) Determination of Nitric oxide (NO) levels

Nitric oxide levels in BALF were determined using Griess reagent [46]. Briefly, to whole lung tissue supernatant, Griess reagent was added in equal proportion and incubated in dark for 5 min. Absorbance was read at 548 nm. The absorbance values were compared with sodium nitrite taken as standard. NO levels were expressed as μM/mg of protein.

(c) Estimation of collagen content (hydroxyproline assay)

Hydroxyproline level in homogenized lung tissues was measured as an index of collagen accumulation. The protocol followed was as per Linjunyawong et al. with slight modifications [47]. Briefly, equal amount of lung tissues were weighed, homogenized and were subjected to acid hydrolysis. Then, chloramine-T was added to carry out oxidation of the tissue homogenates, followed by addition of Ehrlich reagent. Samples were heated at 60 °C for 20 mins, cooled to room temperature and absorbance was read at 550 nm. Concentrations of hydroxyproline in samples were calculated using concentration-absorbance curve of hydroxyproline standard. Results were represented as μg/mg of lung tissue.

(d) Sircol assay (estimation of collagen content by Sirius Red)

Lung tissues were homogenized using Tris Hcl buffer and supernatant was collected. Collagen binding dye was added and incubated for 1 h at 37 °C followed by centrifugation. Supernatant was discarded; visible red pellet was dissolved in 100% ethanol to remove excess dye and centrifuged. Then, obtained pellet was dissolved in 0.5 M sodium hydroxide solution, incubated for 30 min at 37 °C and absorbance was measured at 540 nm using spectrophotometer. Collagen levels so obtained were expressed as μM/mg normalized with lung protein content obtained by Bradford assay as described earlier.

2.11. Histopathological examination

Lung tissues harvested at study termination were fixed in 10% non-buffered formalin. Fixed tissues were processed using gradient alcohols and xylene, subjected to paraffin infiltration followed by embedding of the tissue. Then, embedded tissues were cut into 5 μ thick sections using microtome, mounted on slides and used for further microscopic analysis (as described further) under light microscopy. Haematoxylin and Eosin (H&E) was performed to observe the morphological changes in lung tissues. Mast cell staining (toulidine blue) was performed to estimate the extent of inflammatory cell influx in lung. Picrosirius red staining and Masson's trichrome staining was done to determine the collagen accumulation in lung tissue sections.

2.12. Estimation of inflammatory cytokine levels by ***enzyme linked immunosorbent assay*** *(ELISA)*

Pro-inflammatory cytokines TNF-α, IL-1β and IL-6 in lung tissue supernatants were estimated using ELISA kit based method as per the manufacturers' instructions (e-Biosciences, USA). Results were expressed in pg/mg of protein.

2.13. Immunohistochemical analysis of lung tissue

The paraffin-embedded sections of lung tissue on microscopic slides were deparaffinised in xylene, gradient alcohols and endogenous peroxidase was quenched with 3% H_2O_2. Epitope retrieval was performed by heating sections for 10 min in citrate buffer. Nonspecific reactions were incubated with blocking solution (3% BSA). Then, sections were incubated with primary antibodies and incubated for 30 min at room temperature, followed by incubation with secondary antibody solution for 1 h at room temperature. Tissue sections were then counterstained in haematoxylin, mounted with resinous mounting solution and visualized for immunopositivity [48].

2.14. Western blot analysis

Lung tissues were homogenized in ice-cold lysis buffer centrifuged at 5000 *g* for 10 min. Cells were harvested 24 h post TGF-β1 induction and protein extraction was performed using RIPA (radio immune-precipitation assay buffer) to which protease cocktail mixture & phosphatase inhibitor were added, agitated at high speed three times at 10 min interval. The supernatant was collected after centrifugation at 12,000 rpm for 10 min. Protein concentrations of the supernatants were measured with the BCA protein assay kit. Equal amounts of protein were separated by SDS-PAGE gel and electrophoretically transferred to nitrocellulose or Polyvinylidene difluoride (PVDF) membranes. Then, membranes were blocked with 3% BSA and incubated with specific primary antibodies diluted in TBST at 4 °C overnight. After washing, membrane was incubated with appropriate secondary antibodies. Then protein bands were detected by enhanced chemiluminescence (ECL) reagent. Images were quantified using ImageJ software. The membranes were probed with β-actin antibody as an internal control and to ensure equal loading.

2.15. Immunofluorescence studies

HFL 1 cells were cultured on cover slips and after the cells were confluent enough, cells were treated with NIM followed by TGF-β1 stimulation in presence or absence of autophagy inhibitor chloroquine. 24 h post treatment, cells were fixed with 4% paraformaldehyde for 10 min, washed with PBS and permeabilized with 0.1% Triton X-100 in PBS for about 10 min. Then, cells were washed twice with PBS and incubated for 1 h with 3% BSA blocking. After blocking, cells were incubated with primary antibody p-62 at 1:400 dilutions in 3% BSA overnight at 4 °C.

For processing of lung tissue sections for immunofluorescence, lung sections were deparaffinised for 30 min at 60 °C and treated with xylene and graded alcohols. Then, for antigen retrieval, the lung sections were subjected to citrate buffer for 10 min while heating. Tissue sections were incubated with 3% blocking solution for 30 min at room temperature, immunostained with primary antibodies against Beclin 1 (1:100 dilution) overnight at 4 °C. Then, cells/tissue sections were incubated with Fluorescein isothiocyanate (FITC) anti-rabbit secondary antibody for 2 h at room temperature. Secondary antibody incubation was followed by washing and mounting with vectashield hardset antifade® mounting medium with DAPI (Vector Labs, USA). Intensity of fluorescence in the tissue sections were visualized using confocal microscope (Leica TCS SP8 Laser Scanning Spectral Confocal) [33].

2.16. Statistical analysis

Results of each group were expressed as mean ± standard error of mean (SEM) of three independent experiments and significant differences between means were calculated by one-way analysis of variance (ANOVA). The difference between groups at < 0.05 levels was considered as statistically significant. The intergroup variations were measured by Tukey's multiple comparison tests using the software Graph Pad Prism, Version 5.

3. Results

3.1. NIM inhibits TGF-β1 induced cell proliferation, cell migration and attenuates EMT in both TGF-β1 induced in vitro and BLM induced in vivo PF

Initially, we determined the effect of NIM on viability and proliferation of A549 and HFL 1 cells. Cells were pre-treated with NIM at different concentrations (0.5, 1 and 2 μM) 2 h prior to induction with TGF-β1 at a dose of 10 ng/mL. IC_{50} value of NIM was found to be 7.01 ± 0.12 and 13.81 ± 1.04 μM in A549 and HFL 1 cells respectively 24 h post treatment, studied using MTT assay (Fig. 1A, B). Additionally, we also assessed the anti-fibrotic effect of NIM on TGF-β1 mediated cell migration by performing wound scratch assay. After 24 h of assay, the migration rate of TGF-β1 induced fibroblasts was repressed in a dose dependent manner by NIM, suggesting the inhibitory effect of NIM on TGF-β1 induced cell migration (Fig. 1C, D).

Subsequently, we hypothesized that NIM suitably modulated the expression of EMT markers α-smooth muscle actin (α-SMA), E-cadherin, fibronectin and Zonula occludens (ZO-1) by affecting the fibroblasts differentiation into myofibroblasts, which are a type of specialized contractile cells with higher profibrotic potential. TGF-β1 stimulation in A549 and HFL 1 cells resulted in decreased E-cadherin and ZO-1 expression and was increased α-SMA and fibronectin expression respectively. NIM treatment restored the levels of E-cadherin and ZO-1 in A549 cells and attenuated the expression of α-SMA and fibronectin in HFL 1 cells (Fig. 1E, F). Protein expression of α-SMA was suppressed and E-cadherin was restored upon treatment with NIM dose dependently *in vivo* as well as apparent from western blot analysis. Consistent with protein expression of α-SMA *in vitro* and *in vivo*, immunohistochemical analysis of lung tissue sections revealed dose dependent eloquent reduction in distribution of α-SMA-positive cells by NIM as shown in Fig. 1N. These results suggest that NIM could effectively reverse TGF-β1 and BLM induced EMT events both *in vitro* and *in vivo* respectively by inhibiting transdifferentiation of fibroblasts to myofibroblasts.

3.2. Positive effects of NIM on inflammation, oxidative stress and BALF parameters

Inflammatory response to oropharyngeal aspiration of BLM starts with an acute phase of neutrophil infiltration, gradually increasing the permeability of lung microvasculature, followed by gradual progression to lymphocyte predominant chronic inflammation [20]. Lung/body weight index was significantly increased upon BLM instillation as compared to normal control. Daily administration of NIM significantly decreased lung/body weight index (Fig. 2A, B). A biochemical estimate of the extent of lung injury caused was evaluated by determining the total cell count and differential cell count of lymphocytes, monocytes, leukocytes and neutrophils in BALF. Significant elevation in the total and differential cell count in BALF collected from BLM treated group was noted. NIM decreased the infiltration of lymphocytes, monocytes, leukocytes and neutrophils. This decline in the differential cell count was reflected as a decrease in total cell count in BALF of NIM treated groups compared to BALF from BLM control (Fig. 2B-G). Parallelly, we also estimated the changes in BALF total protein content and levels of lactate dehydrogenase, a cytoplasmic enzyme indicative of cell damage. High total protein and LDH levels in BLM treated group indicated increased pulmonary microvascular albumin permeability, microvascular leakage and elevated LDH indexed the lung damage. NIM at both doses significantly reduced increased levels of total protein and LDH as shown in (Fig. 2H, I).

We further demonstrated the effect of NIM on levels of NF-κB p65 and IL-1β *in vivo* through immunoblotting of HFL 1 cell lysates, where a conspicuous increase in expression of NF-κB p65 and Interleukin-1β (IL-1β), and a dose dependent decrease was observed upon intervention with NIM. Similarly, Interleukin-6 (IL-6) expression in HFL 1 treated cells showed increased expression in TGF-β1 induced cells and was attenuated in the NIM treated cells (Fig. 3A).

Numerous studies have shown ROS to be associated with many interstitial lung diseases and that anti-oxidants are effective in attenuating fibroproliferative responses [21–24]. NIM, being one such potent anti-oxidant, we further aimed at demonstrating, the effect of NIM on oxidative stress. Lung tissue supernatants were evaluated for GSH and NO levels. Prominent decrease in levels of GSH and an expected increase in NO content were observed in BLM treated groups. NIM was shown to exert its anti-oxidant effect by suppressing the levels of NO at both doses. However, NIM treatment restored the levels of GSH only in group treated with high dose. No significant difference was observed in lung homogenates of group treated with low dose of NIM (Fig. 3E, F).

To authenticate the anti-inflammatory effect of NIM, we performed ELISA to determine the levels of prominent pro-inflammatory cytokines TNF-α, IL-1β and IL-6 in lung tissue supernatants. As depicted in Fig. 3G-I, a significant increase in levels of TNF-α, IL-1β and IL-6 in BLM treated lung tissue supernatants was observed which are in agreement with literature. Upregulated levels of the aforementioned pro-inflammatory cytokines were significantly suppressed in the treated groups in dose dependent manner. Toulidine blue staining was performed to determine the extent of distribution of inflammatory cells. In consistent with results of ELISA, high amount of inflammatory cells were observed in BLM treated lung section. NIM dose dependently decreased the inflammatory cells in treated lung sections (Fig. 3J). Thus, from the above array of results obtained, it can be stated that NIM exhibits exceptional anti-inflammatory activity both *in vitro* and *in vivo*.

3.3. NIM strongly limits progressive collagen accumulation

Fibroblast activation contributes to tissue remodelling by secretion and accumulation of collagen [25]. Pathological collagen deposition is one of the distinctive features of fibrosis detrimentally altering lung mechanics [26]. On the grounds of such convincing evidences, we sought to investigate the effect of NIM on deposition of collagen. Firstly, we performed western blot analysis of lung tissue supernatant from which it was evident that collagen subtype 3A1 levels were substantially reduced by NIM concentration dependently (Fig. 4A). Further, hydroxyproline assay and Sircol assay were performed to quantify the collagen content in lung homogenates. Not surprisingly, heightened collagen content was noted in BLM treated group. NIM significantly retarded the collagen deposition in group treated with high dose.

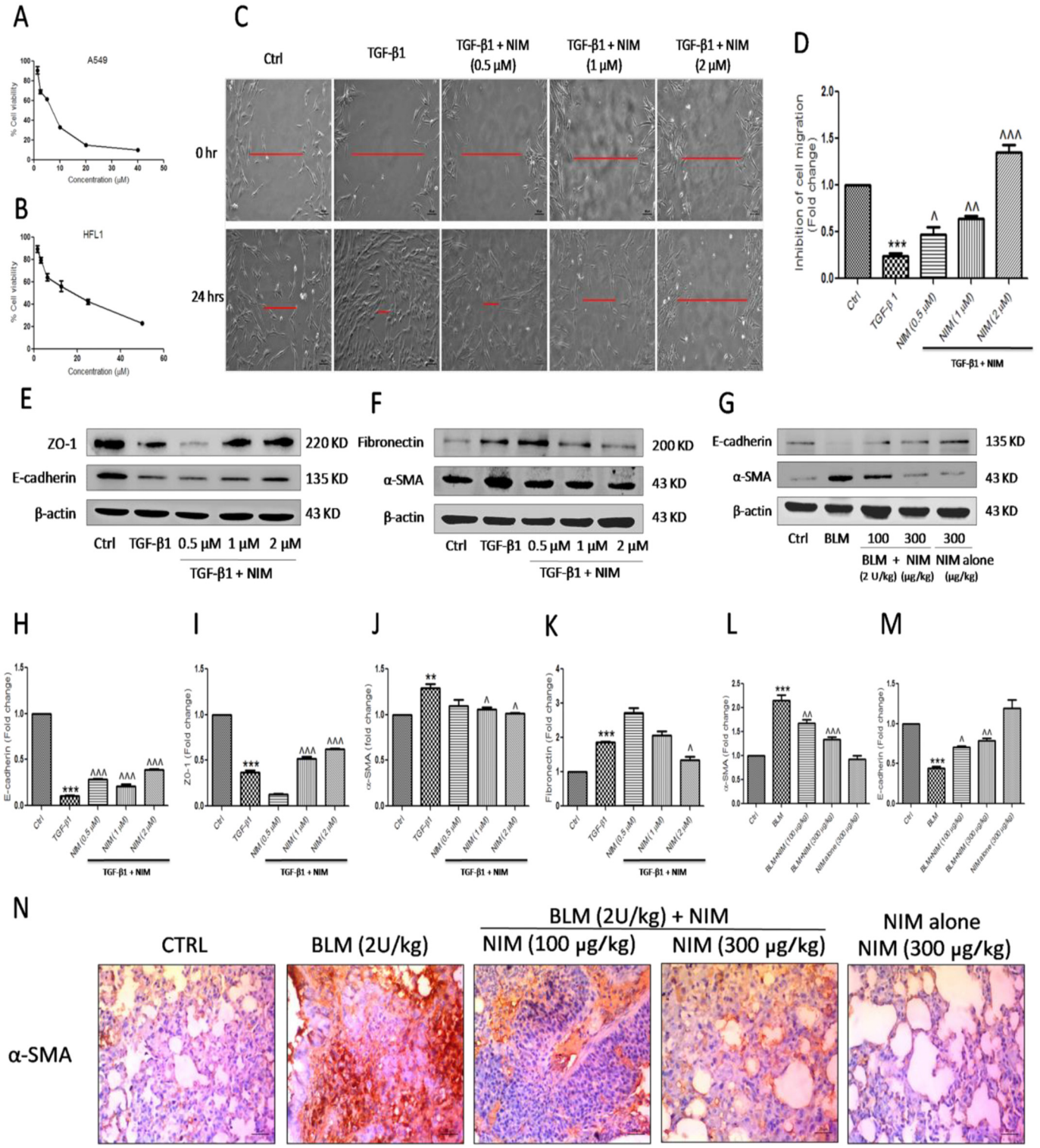

Fig. 1. Effect of NIM on cell viability, cell migration and EMT. HFL 1 cells were treated with NIM at concentrations of 0.5, 1 and 2 μM prior to stimulation with TGF-β1 (10 ng/mL). BLM (2 U/kg) was administered to mice oropharyngeally followed by treatment with NIM at doses of 100 or 300 μg/kg or vehicle (i.p) for 21 days. Effect of NIM on cytotoxicity (A) A549 cells (B) HFL 1 cells (C) Inhibition of cell migration by NIM in HFL 1 cells. Wound closure was photographed at 0 h and 24 h post-scratching. (D) Graphical representation of NIM in regulating wound closure rate. (E) Western blot analysis of EMT markers ZO-1 and E-Cadherin in A549 cell lysates stimulated with TGF-β1. (F) Western blot analysis of mesenchymal markers fibronectin and α-SMA in lysates of HFL 1 cells stimulated with TGF-β. (G) Western blot analysis of epithelial marker E-cadherin and mesenchymal marker α-SMA in lung tissue whole cell lysates. (H,I) Respective densitometric analysis of E-Cadherin and ZO-1 in the immunoblots using β-actin as internal standard. (J, K) Respective densitometric analysis of α-SMA and fibronectin in the immunoblots using β-actin as internal standard. (L, M) Densitometric analysis of α-SMA and E-Cadherin in the immunoblots using β-actin as internal standard. Statistical significance was tested using one-way ANOVA. Data expressed as mean ± SEM, $^{**}p < 0.01$; $^{***}p < 0.001$ of BLM versus Ctrl ; $\hat{}p < 0.05$; $\hat{}\hat{}p < 0.01$; $\hat{}\hat{}\hat{}p < 0.001$ of NIM versus BLM.

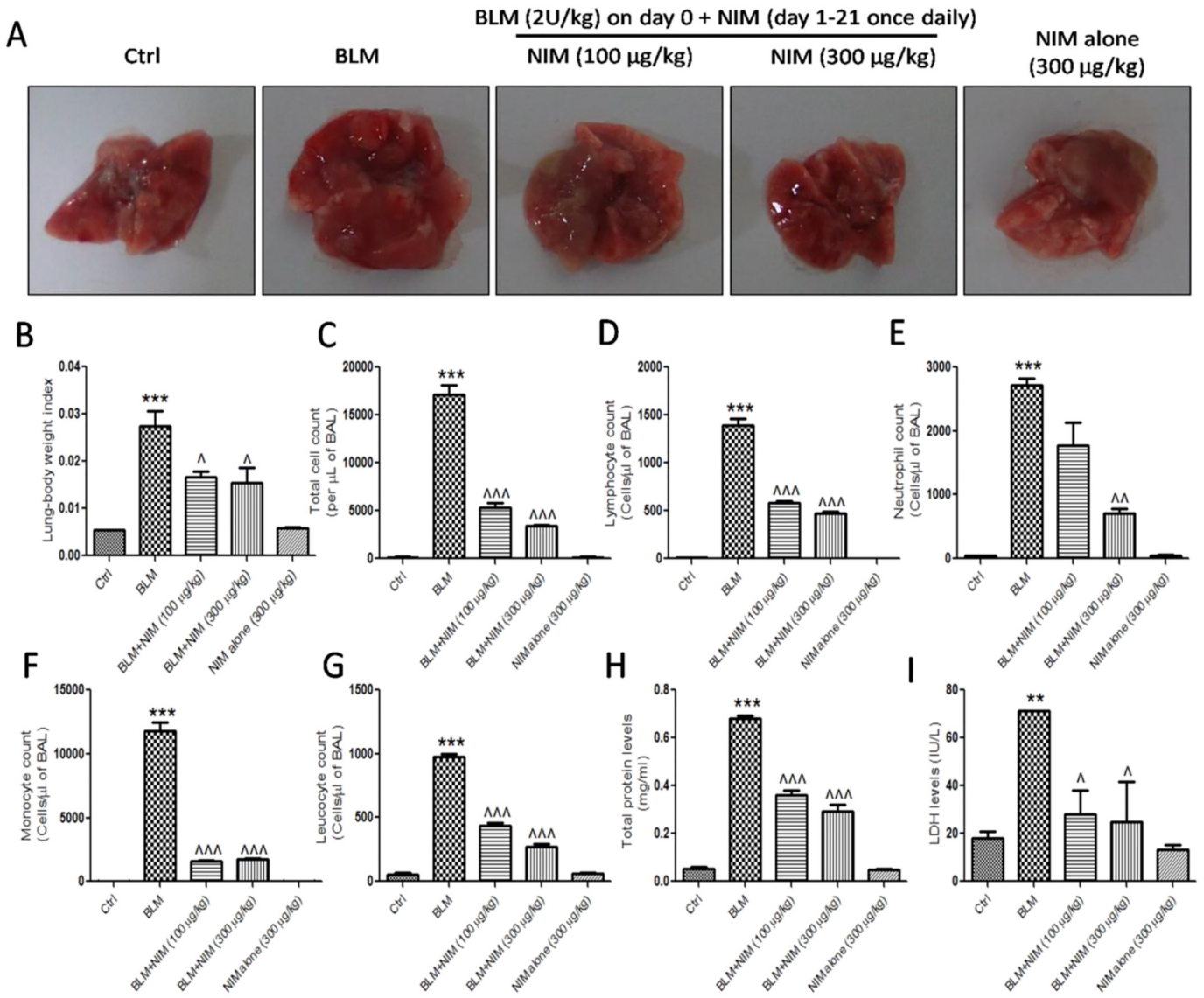

Fig. 2. Effect of NIM on lung morphology, lung-body weight index and BAL biochemical parameters. BLM (2 U/kg on day 0) was administered to mice oropharyngeally followed by treatment with NIM at doses of 100 or 300 µg/kg or vehicle (i.p) from day for 21 days, once daily. (A) Representation of lung images of all the study groups harvested on the day of termination, after 28 days of study. (B) Ratio of lung to body weight index, taking into consideration wet weight of lungs. Effect of NIM on inflammatory cell count estimated in BALF: (C) Total cell count (D) Lymphocytes (E) Neutrophils (F) Monocytes (G) Leucocytes (H) Total protein content (I) LDH levels. Units of differential cell count on Y axis represent number of cells (10 [6]) per µL of BALF. Statistical significance was tested using one-way ANOVA. Data expressed as mean ± SEM, $^{**}p < 0.01$; $^{***}p < 0.001$of BLM versus Ctrl ; $\hat{}p < 0.05$; $\hat{}\hat{}p < 0.01$; $\hat{}\hat{}\hat{}p < 0.001$ of NIM versus BLM.

However, no notable changes with respect to collagen deposition were observed in low dose treated group (Fig. 4C, D). H&E staining indicated disrupted lung architecture in BLM lung tissue sections due to excessive ECM accumulation. NIM restored the lung frame work in dose dependent manner. Then, to quantify extent of collagen accumulation histologically, collagen and elastin fibres were visualized by Masson's trichrome and Picro Sirius red staining. Lung sections from BLM insult group showed more abundant collagen accumulation in alveolar space, at the sites surrounding vascular vessels or bronchioles and abundant regional fibrotic foci. Marked reduction in the regional fibrotic foci and collagen depositions were observed further confirming that NIM limits collagen deposition (Fig. 4E). The above results suggest that NIM retards collagen expression in lung tissues.

3.4. NIM interferes with canonical TGF-β1/Smad Signaling axis in vitro and in vivo

Further, to explore the effect of NIM on basic TGF-β/Smad signaling, we performed protein expression studies for the important components of this interactive pathway. NIM ameliorated the over-expressed phosphorylated Smad2/3 in a dose-dependent manner in HFL 1 cell lysates. NIM also significantly diminished the expression of TGF-β1, which is the most strongly implicated cytokine in progression of PF dose dependently in *in-vitro* studies performed on HFL 1 cells. Connective tissue growth factor (CTGF), a major matricellular protein is one of the pivotal players in fibrosis which was aberrantly expressed upon TGF-β1 induction in HFL 1 cells. Upon treatment with NIM, CTGF expression was declined nearly to normal levels as evident from Fig. 5A.

Confirming the above outcomes, similar results were obtained upon analyses of the proteins involved in TGF-β/Smad signaling cascade by western blotting of lung tissue whole cell lysates. Immunoblotting showed marked elevation of phosphorylated Smad2/3 was noted in BLM treated lungs which was suppressed significantly upon treatment with NIM (Fig. 5B). In addition, immunohistochemical staining revealed that NIM decreased TGF-β1 expression in a dose dependent manner which was up regulated upon BLM administration (Fig. 5G).

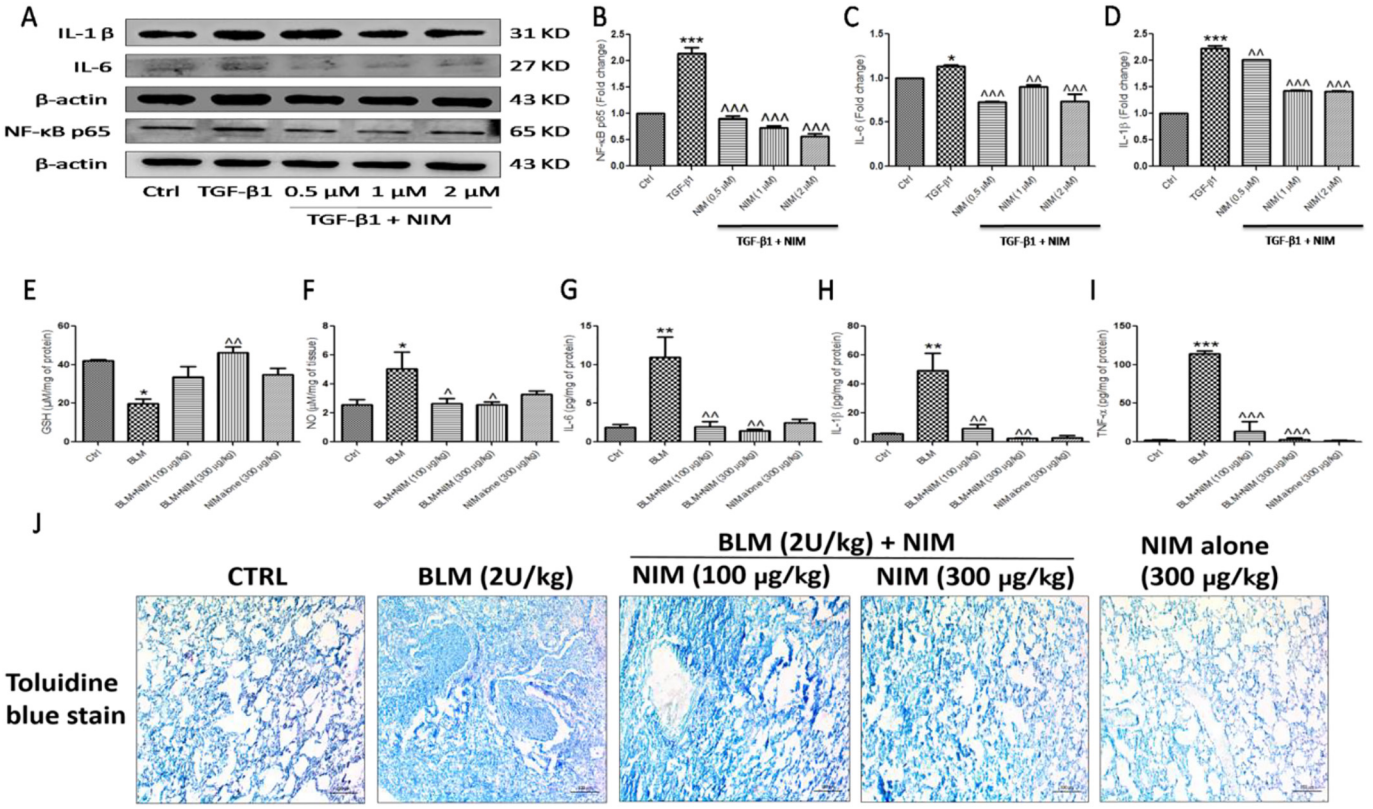

Fig. 3. Effect of NIM on oxidative stress and inflammation. HFL 1 cells were stimulated with TGF-β1 (10 ng/mL) 2 h prior to NIM treatment at concentrations of 0.5, 1 and 2 μM. BLM (2 U/kg) was administered to mice oropharyngeally followed by treatment with NIM at doses of 100 or 300 μg/kg or vehicle (i.p) for 21 days. (A) Western blot analysis of NF-κβ p65, IL-6 and IL-1β in cell lysates. (B-D) Densitometric analysis of NF-κβ p65, IL-6 and IL-1β in immunoblots using β-actin as internal standard. (E) Effect of NIM in elevating glutathione levels (F) Effect of NIM in ameliorating NO content (G-I) Respective ELISA representation of IL-6, IL-1β and TNF-α in lung tissue supernatants. (J) Toluidine blue staining of lung tissue sections. Statistical significance was tested using one-way ANOVA. Data expressed as mean ± SEM, *$p < 0.05$; **$p < 0.01$; ***$p < 0.001$ of BLM versus Ctrl; ^$p < 0.05$; ^^$p < 0.01$; ^^^$p < 0.001$ of NIM versus BLM. (For interpretation of the references to colour in this figure legend, the reader is referred to the web version of this article.)

3.5. Effect of NIM on autophagy signaling

Certain studies in relation to status of autophagy in PF have shown that inhibition of autophagy induces myofibroblast differentiation and contributes to progression of PF [26,27]. To investigate the effect of NIM on regulation of autophagy signaling, we examined the levels of key autophagy markers Beclin 1, Bcl-2, LC-3A/B and p-62. Immunoblotting showed reduced levels of Beclin 1 in TGF-β1 stimulated HFL 1 cells lysates, whereas NIM treatment significantly elevated the expression of Beclin 1. Further, LC-3A/B-I levels were abnormally high in TGF-β1 stimulated HFL 1 cells lysates which were reduced in a dose dependent manner by NIM whereas levels of LC-3A/B-II were nearly equal in all the cell lysates. Thus, ratio of LC-II/LC3-I (lipidated/cytosolic form) levels was diminished in TGF-β1 treated cells. Thereafter, to confirm the above pattern of autophagy protein expression *in vivo*, we performed immunohistochemical analysis of LC-3A/B and p-62, another major partaker in autophagy regulation, in lung tissue sections. In consistent with the LC-3A/B results of western blotting, we performed immunohistochemistry of LC-3A/B. A significant increase in the levels of the cytosolic form of LC-3A/B in BLM treated lung tissues was noted which were visualized as distinct positive signals in cytoplasm Fig. 6 which was reversed upon NIM treatment. Immunohistochemistry of p-62 revealed significant increase of p-62 distribution in the BLM control lung sections. NIM demonstrated dose dependent decrease in distribution of p-62 positive signals. Western blotting analysis of Beclin 1 and Bcl-2 proteins *in vivo* showed decreased expression in BLM treated tissues which were restored upon treatment with NIM. For further affirmation of the results obtained with respect to autophagy regulation, confocal microscopic imaging of Beclin 1 was performed in lung sections. Substantiating, the above evidence, we found diminished expression of Beclin 1 in lung tissues of BLM instilled group. NIM was found to up regulate the expression of Beclin 1 in treated group (Fig. 6). Then, we assessed the influence of NIM on formation of autophagy puncta (autophagic vacuoles) by monodansylcadaverine (MDC) and acridine orange staining techniques in HFL 1 cells. MDC staining revealed the ability of NIM to increase the MDC labelled vesicles in cytoplasm and perinuclear regions in TGF-β1 treated cells. Similarly, formation of autophagic vacuoles were reflected by orange fluorescence which was found to be tremendously increased in cells treated with NIM as evident from acridine orange staining implying autophagy stimulation by NIM (Fig. 7A,B). Finally, we measured autophagy flux by evaluating the levels of p-62 through immunoflouroscence. We found that NIM was capable of decreasing the levels of p-62 in presence of TGF-β1 as well as both TGF-β1 and classical autophagy inhibitor chloroquine (CQ) as evident from the percentage decrease in intensities (Fig. 7C, D).

4. Discussion

Regardless of advancement in research with respect to PF till date, managing this life threatening pulmonary disorder persists as a clinical challenge [28,29]. Lacunae in the existing therapies for PF and their adverse effects [30] impelled us to explore the potential of NIM in TGF-β1 induced *in vitro* and BLM induced *in vivo* model of PF. Our study was oriented at demonstrating the anti-fibrotic effects of NIM, a chief constituent of *Azadirachta indica* (neem) which is considered as the panacea

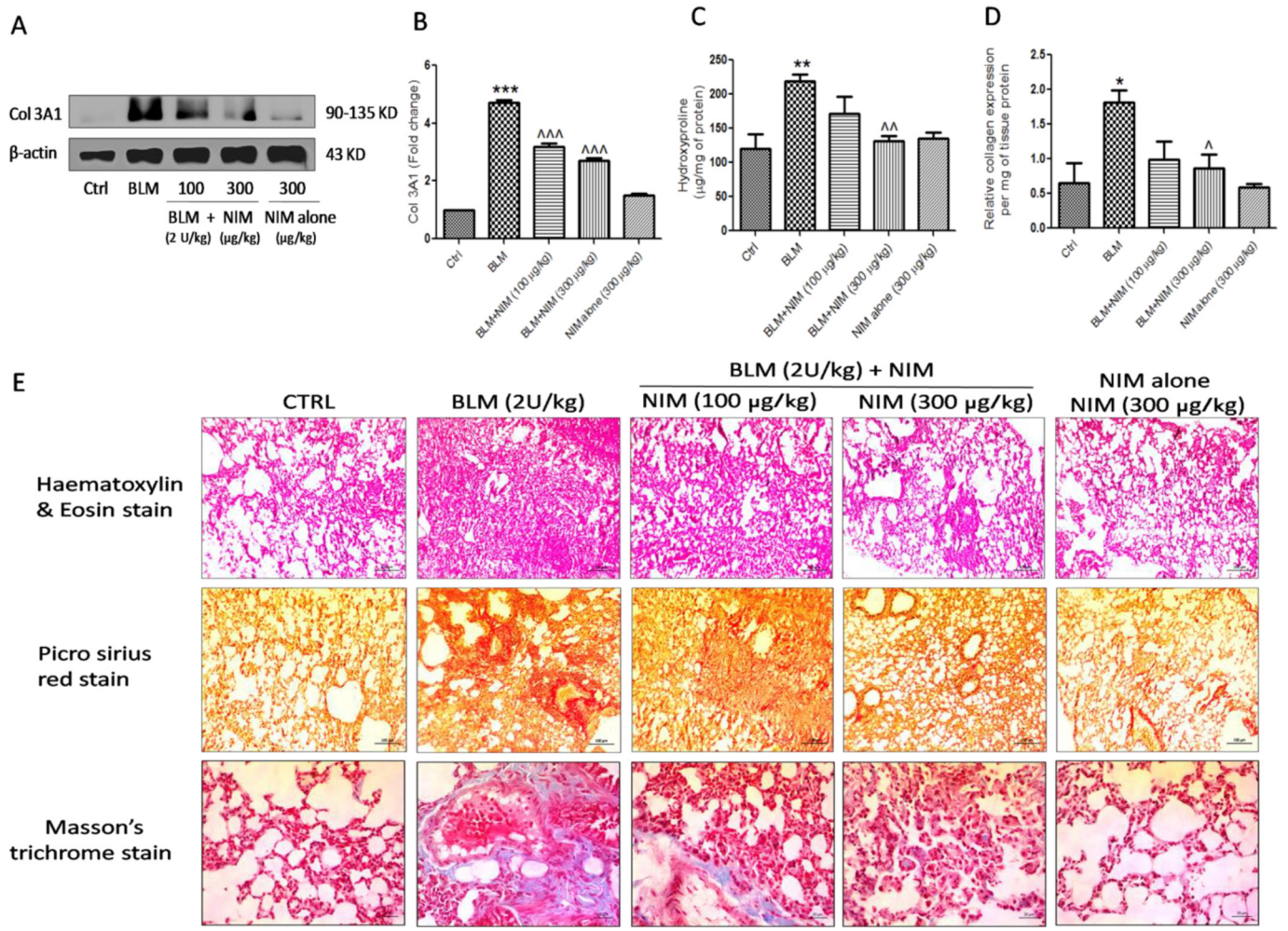

Fig. 4. Effect of NIM in ameliorating excess collagen deposition. BLM (2 U/kg) was administered to mice oropharyngeally followed by treatment with NIM at doses of 100 or 300 μg/kg or vehicle (i.p) for 21 days. (A) Western blot analysis of collagen 3A1 in lung tissues. (B) Densitometric analysis of Collagen 3A1 in immunoblot using β-actin as internal standard. (C) Estimation of hydroxyproline content in lung tissues as an index of collagen deposition. Data expressed as μg/mg of protein. (D) Estimation of soluble collagen content using Sircol assay (E) staining of lung tissue sections using H&E for lung architecture, Picrosirius red for collagen deposition; (magnification 100 X) and Masson's trichrome staining of lung tissue sections to estimate collagen (magnification 400 X). Statistical significance was tested using one-way ANOVA. Data expressed as mean ± SEM, $^{*}p < 0.05$; $^{**}p < 0.01$; $^{***}p < 0.001$ of BLM versus Ctrl; $^{\wedge}p < 0.05$; $^{\wedge\wedge}p < 0.01$; $^{\wedge\wedge\wedge}p < 0.001$ of NIM versus BLM. (For interpretation of the references to colour in this figure legend, the reader is referred to the web version of this article.)

for many diseases as per Indian traditional medicine [31]. This study demonstrates the potential of NIM as anti-fibrotic agent against both well-established TGF-β1 induced *in vitro* and BLM induced *in vivo* experimental models. NIM was administered 2 h prior to TGF-β1 stimulation in *in-vitro* studies where as NIM was administered one day after induction of BLM in *in-vivo* studies as per our established experimental models and in consideration with various literature findings [32,33]. Our findings demonstrated that NIM alleviates PF by attenuating EMT, inflammation, collagen deposition, TGF-β/Smad signaling and fibrosis related autophagy.

Firstly, we determined the cytotoxicity of NIM on HFL 1 and A549 cells, based on which 0.5, 1 and 2 μM were selected as suitable concentrations for further investigations *in vitro*. PF occurs as a result of recurrent epithelial cell injury consequently causing activation of fibroblast migration/proliferation [34]. Thus, we examined the effect of NIM on cell migration and proliferation. A dose dependent inhibition of cell proliferation and migration was observed from cell migration assay performed in HFL 1 cells. Convincing studies on cancer have shown NIM to be potent inhibitor of EMT which is also a dominant pathway governing pathogenesis of PF [16,18]. To gain insight about the underlying mechanisms by which NIM attenuated EMT, we investigated EMT related changes *in vitro* in human type II alveolar epithelial A549 and lung fibroblast HFL 1 cells due to predominant EMT occurrence in both the cell lines. While, whole fibrotic events were explored only in HFL 1 cells due to inherent lung matrix homeostasis. Presence of TGF-β1 compels epithelial cells to transform rapidly into mesenchymal cells, then into fibroblasts and, eventually to myofibroblasts [35]. As EMT progresses, loss of E-cadherin and ZO-1 takes place. In contrast, an increase in α-SMA and fibronectin, biomarkers of myofibroblasts occurs [36]. Relevant EMT changes were induced by pro-fibrotic cytokine human recombinant TGF-β1 in A549 and HFL 1 cells. NIM treatment in TGF-β1 stimulated not only reinstated expression of important epithelial markers E-cadherin and ZO-1 but also adequately decreased α-SMA and fibronectin levels in A549 cells and HFL 1 cells respectively. This implies that NIM inhibits various stages in the process of EMT. Similarly epithelial marker E-cadherin was restored and mesenchymal marker α-SMA was down-regulated in lung tissues, which reflected that EMT is substantially attenuated by NIM both *in vitro* and *in vivo*.

NF-κB, a crucial inflammatory cytokine is a redox-sensitive transcription factor activated by ROS [37]. Sensing the importance of NF-κB/ROS cross talk in PF, we evaluated the expression of inflammatory proteins. In concurrence with existing literature, we found high expression of NF-κB p65, IL-1β and IL-6 *in vitro*. NIM being a potent anti-inflammatory active constituent was able to regulate the expression of

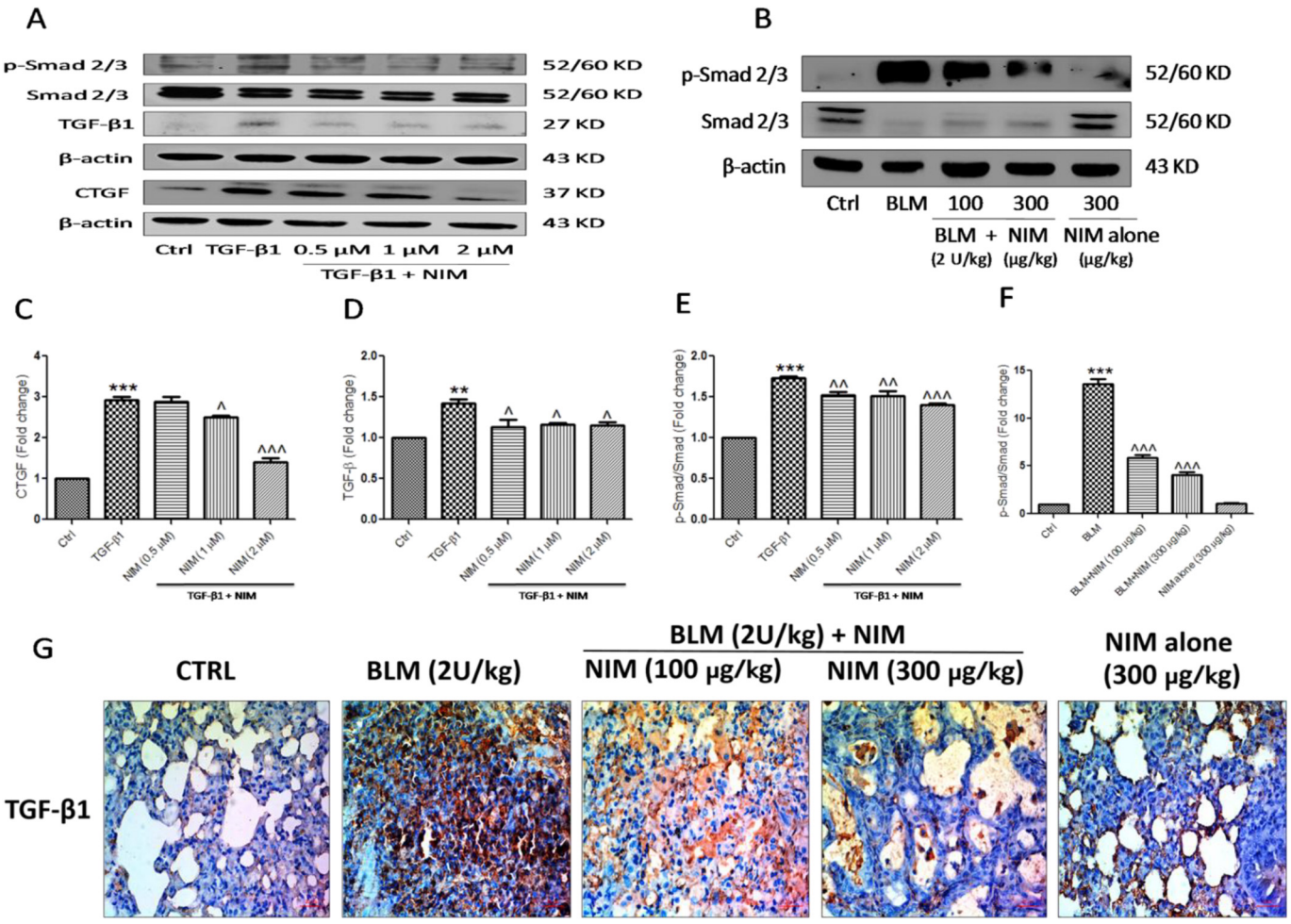

Fig. 5. Amelioration of Smad-dependent TGF-β1 signaling by NIM. HFL 1 cells were stimulated with TGF-β1 (10 ng/mL) 2 h prior to NIM treatment at concentrations of 0.5, 1 and 2 μM. BLM (2 U/kg) was administered to mice oropharyngeally followed by treatment with NIM at doses of 100 or 300 μg/kg or vehicle (i.p) for 21 days. (A) Western blot analysis of CTGF, TGF-β, Smad 2/3 and p-Smad 2/3 in cell lysates of TGF-β1 induced HFL 1 cells. (B) Western blot analysis of Smad 2/3 and p-Smad 2/3 in lung tissues. (C-E) Respective densitometric analysis of *in vitro* CTGF, TGF-β1, and p-Smad/Smad in immunoblot using β-actin as internal standard. F) Respective densitometric analysis of *in vivo* p-Smad/Smad in immunoblot using β-actin as internal standard. (G) Immunohistochemical staining of TGF-β1 positive cells in lung tissue sections (magnification 400 X). Statistical significance was tested using one-way ANOVA, $^{**}p < 0.01$; $^{***}p < 0.001$ of BLM versus Ctrl; $^{\wedge}p < 0.05$; $^{\wedge\wedge}p < 0.01$; $^{\wedge\wedge\wedge}p < 0.001$ of NIM versus BLM.

pro-inflammatory cytokines. Credibility of NIM as an anti-inflammatory agent was further established by reduced levels of NO associated with restoration of GSH levels. Further, NIM ameliorated the expression of pro-inflammatory markers including IL-6, IL-1β and TNF-α as evident from ELISA reflecting the potential of NIM as an anti-inflammatory agent. Decreased inflammatory cells influx in lung tissue sections of treatment groups as noted in toulidine blue staining and diminishing count of inflammatory cells of BALF from NIM treated animal lungs further confirms the anti-inflammatory effect of NIM with respect to histological and biochemical perspectives respectively. Subsided total protein and LDH content upon NIM administration in mice reflects the ability of NIM to reduce BLM induced vascular leakage of proteins due to altered permeability.

TGF-β1 induction promotes pro-fibrotic gene activation resulting in excessive secretion and deposition of interstitial matrix, thickening of alveolar walls and thus disrupting the alveolar framework [34,38]. To study the effect of NIM on TGF-β1 and its downstream fibrotic signaling, we used Human recombinant TGF-β1, a well-known inducer of fibrosis to stimulate PF in lung fibroblast HFL 1 cells. TGF-β1 treatment induced fibrosis in HFL 1 cells and NIM effectively decreased the expression of fibrotic markers such as CTGF and fibronectin as observed from the results of western blot analysis. Additionally, immunoblotting indicated that NIM inhibited phosphorylation of Smad 2/3 *in vitro*. In agreement with the *in vitro* fibrotic protein expression results, NIM significantly regulated the TGF-β/Smad signaling *in vivo* in experimental model of BLM induced PF. As evident from various literature reports, over expression of TGF-β1 induced pro-fibrotic CTGF expression mediates the up regulation of collagen deposition and dramatic thickening of perivascular regions of the lungs [34,39,40]. A prominent decrease in collagen expression was observed upon treatment with NIM that was reflected from *in vivo* immunoblot of Col 3A1, which was consistent with reduced lung/body weight index by NIM as evident from macroscopic findings. Microscopic evidence was accumulated by Masson's trichrome and Sirius red tissue staining. Also, NIM was capable of sharply decreasing the increased levels of hydroxyproline *in vivo*. This was also evident from the results of Sircol assay. These results satisfactorily convince that abnormal collagen accumulation was blocked by NIM.

Autophagy is a multifaceted signaling cascade involving various proteins of diverse functions [41]. Mounting evidence displays role of autophagy in pathogenesis of PF as ambiguous with few sources stating it as a contributor to pathology of PF and certain other reports stating it to be otherwise. In the present study, we determined the role of NIM in regulating autophagy proteins Beclin 1, LC-3A/B-I/II and p-62 through

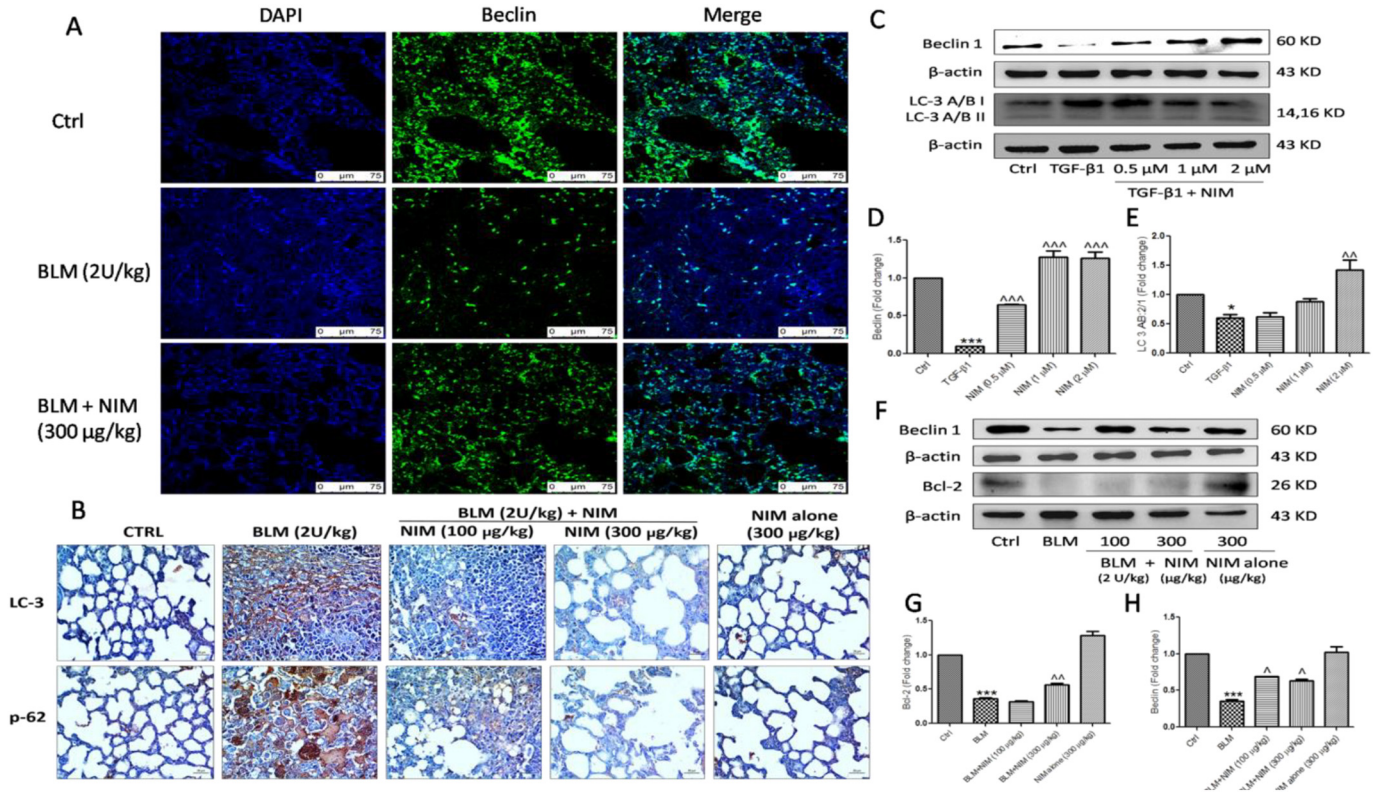

Fig. 6. Modulation of autophagy by NIM *in vitro* and *in vivo*. HFL 1 cells were stimulated with TGF-β1 (10 ng/mL) 2 h prior to NIM treatment at concentrations of 0.5, 1 and 2 µM. BLM (2 U/kg) was administered to mice oropharyngeally followed by treatment with NIM at doses of 100 or 300 µg/kg or vehicle (i.p) for 21 days. (A) Immunofluoresence staining of Beclin 1 (autophagy protein) performed on lung tissue sections using confocal microscopy. (B) Immunohistochemical staining of LC-3 and p-62 (autophagy proteins) positive cells in lung tissue sections (magnification 400×). (C) Western blot analysis of autophagy markers LC-3 and Beclin 1 in HFL 1 whole cell lysates. (D, E) Densitometric analysis of Beclin 1 and LC-3 in the immunoblots using β-actin as internal standard. (F) Western blot analysis of autophagy markers Bcl-2 and Beclin 1 in lung tissue whole cell lysates. (G, H) Densitometric analysis of Bcl-2 and Beclin 1 in the immunoblots using β-actin as internal standard. Statistical significance was tested using one-way ANOVA, *$p < 0.05$; ***$p < 0.001$ of BLM versus Ctrl; ^$p < 0.05$; ^^$p < 0.01$; ^^^$p < 0.001$ of NIM versus BLM.

various protein expression studies. Significant down regulation of Beclin 1 and Bcl-2, which are central proteins in the process of autophagy was noted *in vivo* immunoblotting studies. To further confirm its role in PF and how NIM regulated Beclin 1, we performed immunofluorescence of Beclin 1 in lung tissue sections, the result of which was consistent with the immunoblot. Reduced Beclin 1 expression upon BLM challenge implies decrease in autophagy induction and increased p-62 and LC-3A/B levels implicate impaired autophagosome formation and clearance. Confocal imaging showed faintly detectable immunofluorescence of BLM treated lung sections where as NIM treated lung sections showed increased immunoreactivity implying NIM up regulated Beclin 1 expression. Dampening distribution of LC-3A/B and p-62 positive immune reactive signals in NIM treated lung tissues as compared to the BLM control was obvious. Treatment with NIM enhanced autophagy vacuoles in perinuclear regions of TGF-β1 stimulated HFL 1 cells as evident from MDC and acridine orange staining techniques. As p-62 protein is degraded through autophagy, its expression can serve as a marker of autophagic flux. Expression of p-62 protein has a direct negative correlation with autophagic flux as stated by Min et al. [42]. NIM significantly dissipated the expression of p-62 in both TGF-β1 treated cells and also in cells which received a combination of TGF-β1 and chloroquine indicating that autophagy flux was altered by NIM. These observations with respect to regulation of autophagy proteins imply that NIM stimulates autophagy.

In conclusion, *in vitro* and *in vivo* assays performed in the present study sufficiently demonstrate NIM as a very promising anti-fibrotic molecule which impedes EMT pathway, reasonably blocks TGF-β/Smad and its downstream signaling events, thus inhibiting collagen deposition and substantially modulates major proteins involved in autophagy signaling cascade. Further understanding of the precise mechanisms of NIM is required. Our study prompts research on use of natural products like NIM with favourable safe properties as pharmacological intervention for PF.

Acknowledgements

The authors acknowledge Anil Kumar Kalvala for his kind support and technical assistance in confocal imaging.

Funding

This study was supported financially by Department of pharmaceuticals, Ministry of chemicals and fertilizers, Government of India. The authors would like to thank DST-Science and Engineering Board-Early Career Research Award (SERB-ECR) Grant: ECR/2016/000007

Author contributions

PGM and SB contributed equally to this work. CG, PGM and SB designed the research work. PGM, SB and PG performed the research. CG, PG and SB wrote the manuscript. All authors reviewed the final version of the manuscript.

Declaration of Competing Interest

The authors declare no conflict of interest.

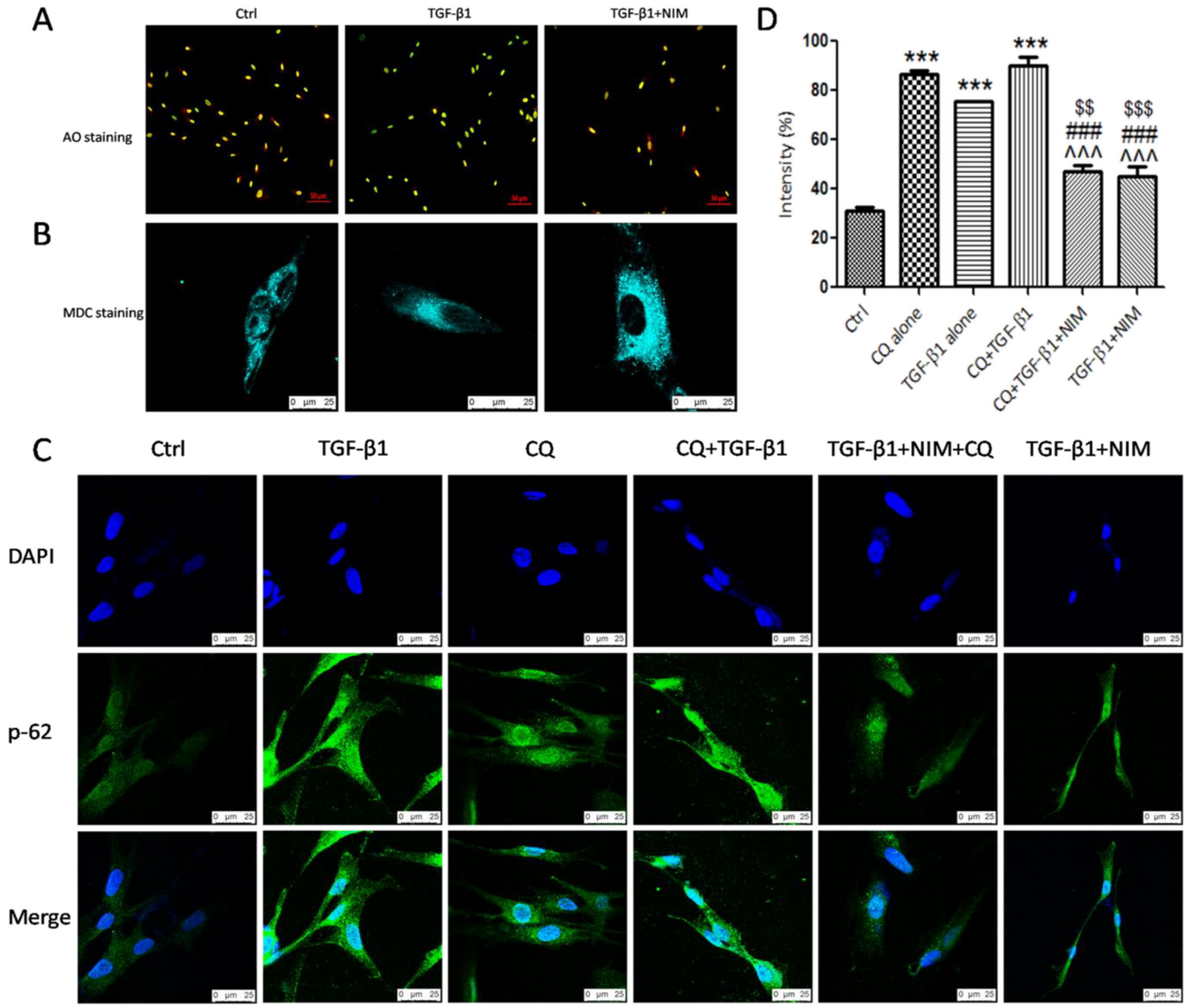

Fig. 7. Autophagy regulation by NIM *in vitro*. (A, B) AO and MDC stainings demonstrating the stimulation of autophagy by NIM. (C) Immunocytochemistry eliciting the role of NIM on p-62 expression. HFL 1 cells treated with TGF-β1 demonstrated elevated expression of p-62. NIM at a concentration of 2 μM ameliorated the expression of p-62 in the presence of TGF-β1. Further NIM reduced the expression of p-62, a negative regulator of autophagy flux compared to chloroquine (CQ) alone group suggesting the altered autophagy flux by NIM (D) Graphical representation of percentage intensity of p-62 fluorescence signal in different experimental groups *in vitro*. *** indicates Ctrl *vs* TGF-β1, ^^^ indicates CQ *vs* NIM treated groups, ### indicates CQ + TGF-β1vs NIM treated groups, $$$ indicates TGF-β1 *vs* NIM treated groups.

Appendix A. Supplementary data

Supplementary data to this article can be found online at https://doi.org/10.1016/j.intimp.2019.105755.

References

[1] R. Du Bois, A. Wells, Cryptogenic fibrosing alveolitis/idiopathic pulmonary fibrosis, Eur. Respir. J. 18 (2001) 43s–55s.
[2] R.S. Nho, V. Polunovsky, Translational control of the fibroblast-extracellular matrix association: an application to pulmonary fibrosis, Translation 1 (2013) e23934.
[3] E.B. Meltzer, P.W. Noble, Idiopathic pulmonary fibrosis, Orphanet J. Rare Dis. 3 (8) (2008).
[4] J. Egan, F. Martinez, A. Wells, T. Williams, Lung Function Estimates in Idiopathic Pulmonary Fibrosis: The Potential for a Simple Classification, BMJ Publishing Group Ltd, 2005.
[5] R. Guan, X. Wang, X. Zhao, et al., Emodin ameliorates bleomycin-induced pulmonary fibrosis in rats by suppressing epithelial-mesenchymal transition and fibroblast activation, Sci. Rep. 6 (2016) 35696.
[6] B. Ley, H.R. Collard, T.E. King Jr, Clinical course and prediction of survival in idiopathic pulmonary fibrosis, Am. J. Respir. Crit. Care Med. 183 (2011) 431–440.
[7] M.A. Taylor, J.G. Parvani, W.P. Schiemann, The pathophysiology of epithelial-mesenchymal transition induced by transforming growth factor-β in normal and malignant mammary epithelial cells, J. Mammary Gland Biol. Neoplasia 15 (2010) 169–190.
[8] C. Neuzillet, A. de Gramont, A. Tijeras-Raballand, et al., Perspectives of TGF-β inhibition in pancreatic and hepatocellular carcinomas, Oncotarget 5 (2014) 78.
[9] R. Derynck, Y.E. Zhang, Smad-dependent and Smad-independent pathways in TGF-β family signalling, Nature 425 (2003) 577.
[10] A. Datta, C.J. Scotton, R.C. Chambers, Novel therapeutic approaches for pulmonary fibrosis, Br. J. Pharmacol. 163 (2011) 141–172.
[11] A.S. Patel, L. Lin, A. Geyer, et al., Autophagy in idiopathic pulmonary fibrosis, PLoS One 7 (2012) e41394.
[12] K. Mizumura, S. Cloonan, M.E. Choi, et al., Autophagy: friend or foe in lung disease? Annals of the American Thoracic Society 13 (2016) (S40-S7).
[13] V. Hernández-Gea, S.L. Friedman, Autophagy fuels tissue fibrogenesis, Autophagy 8 (2012) 849–850.
[14] P. Chitra, G. Saiprasad, R. Manikandan, G. Sudhandiran, Berberine inhibits Smad and non-Smad signaling cascades and enhances autophagy against pulmonary fibrosis, J. Mol. Med. 93 (2015) 1015–1031.
[15] K. Singh, Neem, A Treatise, IK International Pvt Ltd., 2008.

[16] P. Elumalai, D. Gunadharini, K. Senthilkumar, et al., Induction of apoptosis in human breast cancer cells by nimbolide through extrinsic and intrinsic pathway, Toxicol. Lett. 215 (2012) 131–142.
[17] P. Elumalai, J. Arunakaran, Review on molecular and chemopreventive potential of nimbolide in cancer, Genome Inform. 12 (2014) 156–164.
[18] R. Subramani, E. Gonzalez, A. Arumugam, et al., Nimbolide inhibits pancreatic cancer growth and metastasis through ROS-mediated apoptosis and inhibition of epithelial-to-mesenchymal transition, Sci. Rep. 6 (2016) 19819.
[19] P. Elumalai, R. Arunkumar, C.S. Benson, G. Sharmila, J. Arunakaran, Nimbolide inhibits IGF-I-mediated PI3K/Akt and MAPK signalling in human breast cancer cell lines (MCF-7 and MDA-MB-231), Cell Biochem. Funct. 32 (2014) 476–484.
[20] J. Hay, S. Shahzeidi, G. Laurent, Mechanisms of bleomycin-induced lung damage, Arch. Toxicol. 65 (1991) 81–94.
[21] P. Cheresh, S.-J. Kim, S. Tulasiram, D.W. Kamp, Oxidative stress and pulmonary fibrosis, Biochim. Biophys. Acta (BBA) - Mol. Basis Dis. 1832 (2013) 1028–1040.
[22] F. Jiang, G.-S. Liu, G.J. Dusting, E.C. Chan, NADPH oxidase-dependent redox signaling in TGF-β-mediated fibrotic responses, Redox Biol. 2 (2014) 267–272.
[23] A. Andersson-Sjöland, J.C. Karlsson, K. Rydell-Törmänen, ROS-induced endothelial stress contributes to pulmonary fibrosis through pericytes and Wnt signaling, Lab. Investig. 96 (2016) 206.
[24] B.J. Day, Antioxidants as potential therapeutics for lung fibrosis, Antioxid. Redox Signal. 10 (2008) 355–370.
[25] C. Bonnans, J. Chou, Z. Werb, Remodelling the extracellular matrix in development and disease, Nat. Rev. Mol. Cell Biol. 15 (2014) 786.
[26] I.E. Fernandez, O. Eickelberg, New cellular and molecular mechanisms of lung injury and fibrosis in idiopathic pulmonary fibrosis, Lancet 380 (2012) 680–688.
[27] M.L. Sosulski, R. Gongora, S. Danchuk, C. Dong, F. Luo, C.G. Sanchez, Deregulation of selective autophagy during aging and pulmonary fibrosis: the role of TGFβ1, Aging Cell 14 (2015) 774–783.
[28] K. Ask, G.E. Martin, M. Kolb, J. Gauldie, Targeting genes for treatment in idiopathic pulmonary fibrosis: challenges and opportunities, promises and pitfalls, Proc. Am. Thorac. Soc. 3 (2006) 389–393.
[29] V. Tzilas, A. Tzouvelekis, S. Chrysikos, S. Papiris, D. Bouros, Diagnosis of idiopathic pulmonary fibrosis “pragmatic challenges in clinical practice”, Front. Med. 4 (2017) 151.
[30] G. Hughes, H. Toellner, H. Morris, C. Leonard, N. Chaudhuri, Real world experiences: pirfenidone and nintedanib are effective and well tolerated treatments for idiopathic pulmonary fibrosis, J. Clin. Med. 5 (2016) 78.
[31] R. Subapriya, S. Nagini, Medicinal properties of neem leaves: a review, Curr. Med. Chem. Anticancer Agents 5 (2005) 149–156.
[32] T. Chen, S. Chang, T. Wang, Moxifloxacin modifies corneal fibroblast-to-myofibroblast differentiation, Br. J. Pharmacol. 168 (2013) 1341–1354.
[33] S. Bale, P. Venkatesh, M. Sunkoju, C. Godugu, An adaptogen: Withaferin A ameliorates in vitro and in vivo pulmonary fibrosis by modulating the interplay of fibrotic, matricelluar proteins, and cytokines, Front. Pharmacol. 9 (2018) 248.
[34] N. Khalil, R.N. O'Connor, K.C. Flanders, H. Unruh, TGF-beta 1, but not TGF-beta 2 or TGF-beta 3, is differentially present in epithelial cells of advanced pulmonary fibrosis: an immunohistochemical study, Am. J. Respir. Cell Mol. Biol. 14 (1996) 131–138.
[35] D.C. Rockey, P.D. Bell, J.A. Hill, Fibrosis—a common pathway to organ injury and failure, N. Engl. J. Med. 372 (2015) 1138–1149.
[36] R. Kalluri, E.G. Neilson, Epithelial-mesenchymal transition and its implications for fibrosis, J. Clin. Invest. 112 (2003) 1776–1784.
[37] S. Nakajima, M. Kitamura, Bidirectional regulation of NF-κB by reactive oxygen species: a role of unfolded protein response, Free Radic. Biol. Med. 65 (2013) 162–174.
[38] B.C. Willis, Z. Borok, TGF-β-induced EMT: mechanisms and implications for fibrotic lung disease, Am. J. Phys. Lung Cell. Mol. Phys. 293 (2007) (L525-L34).
[39] S. Wu, A. Platteau, S. Chen, G. McNamara, J. Whitsett, E. Bancalari, Conditional overexpression of connective tissue growth factor disrupts postnatal lung development, Am. J. Respir. Cell Mol. Biol. 42 (2010) 552–563.
[40] Q. Wang, W. Usinger, B. Nichols, et al., Cooperative interaction of CTGF and TGF-β in animal models of fibrotic disease, Fibrogenesis Tissue Repair 4 (2011) 4.
[41] B. Levine, D.J. Klionsky, Development by self-digestion: molecular mechanisms and biological functions of autophagy, Dev. Cell 6 (2004) 463–477.
[42] Z. Min, Y. Ting, G. Mingtao, et al., Monitoring autophagic flux using p62/SQSTM1 based luciferase reporters in glioma cells, Exp. Cell Res. 363 (1) (2017) 84–94.
[43] D.K. Maurya, N. Nandakumar, T.P.A. Devasagayam, Anticancer property of gallic acid in A549, a human lung adenocarcinoma cell line, and possible mechanisms, J. Clin. Biochem. Nutr. 48 (2010) 85–90.
[44] M. Koul, A. Kumar, R. Deshidi, et al., Cladosporol A triggers apoptosis sensitivity by ROS-mediated autophagic flux in human breast cancer cells, BMC Cell Biol. 18 (2017) 26.
[45] M.S. Moron, J.W. Depierre, B. Mannervik, Levels of glutathione, glutathione reductase and glutathione S-transferase activities in rat lung and liver, Biochim. Biophys. Acta Gen. Subj. 582 (1979) 67–78.
[46] I. Guevara, J. Iwanejko, A. Dembińska-Kieć, et al., Determination of nitrite/nitrate in human biological material by the simple Griess reaction, Clin. Chim. Acta 274 (1998) 177–188.
[47] N. Limjunyawong, W. Mitzner, M.R. Horton, A mouse model of chronic idiopathic pulmonary fibrosis, Physiol. Rep. 2 (2014) e00249.
[48] C. Godugu, R. Doddapaneni, M. Singh, Honokiol nanomicellar formulation produced increased oral bioavailability and anticancer effects in triple negative breast cancer (TNBC), Colloids Surf. B: Biointerfaces 153 (2017) 208–219.